

Search for dark matter production in association with top quarks in the dilepton final state at $\sqrt{s} = 13$ TeV

Pablo Martínez Ruíz del Árbol, Jónatan Piedra Gomez, Cédric Prieëls
February 22th 2021

Instituto de Física de Cantabria

- Introduction
- The dark matter case
- The experimental setup
 - The LHC accelerator
 - The CMS detector
- Global strategy
- Data, signals and backgrounds
- Event selection
- Signal extraction
- Systematic uncertainties
- Results and interpretation
- Conclusions

Introduction

A search for the production of dark matter particles in association with either one or two top quarks is presented:

- We study the pp collisions produced by the LHC at $\sqrt{s} = 13$ TeV;
- Reconstruction performed by the CMS detector;
- Legacy analysis, considering the full Run II dataset (data collected in 2016, 2017 and 2018 and summing around 137 fb^{-1}).

Motivation

- Several (mostly astrophysical) evidences for the existence of dark matter, but **no direct nor direct detection** so far;
- We hope to be able to produce such particles in the high energy collisions produced by the LHC if they exist.

Main objective

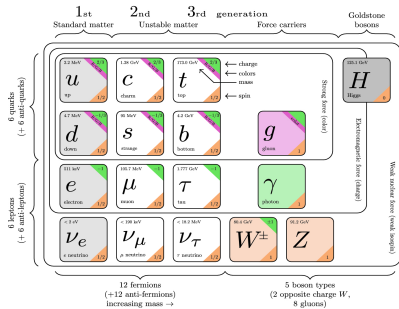
- Consider different dark matter production models to eventually exclude some of them or at least **put upper limits on their cross section of production**.

The dark matter case

The Standard Model

The most accepted model to describe the elementary particles and some of the fundamental interactions between them is the **Standard Model**:

- Contains 26 free parameters, among which the masses of the **12 predicted fermions**;
- Many **successful predictions** made over the years, such as the existence of the top quark, and the W, Z and Higgs bosons [1].



However, this model **has several shortcomings**: eventual exotic particles which do not fit within this model (such as dark matter) are extensively searched for nowadays.

At the origins of dark matter I

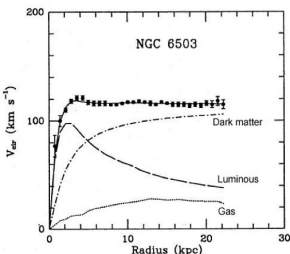
The concept of dark matter can be traced back to the 19th century, and was introduced to **explain several astrophysical evidences**, among which:

Zwicky's calculations

- Measurement of the mass of the Coma Cluster using the virial theorem;
- Concluded that its mass was **400-500 times larger** than the value obtained by Hubble, considering only visible galaxies [2].

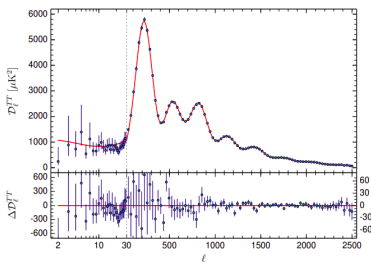
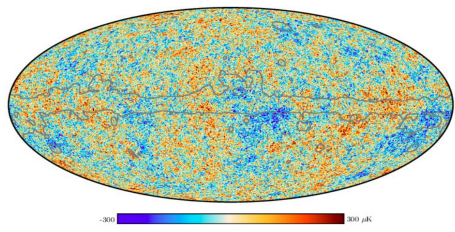
Spiral galaxies rotation curves

- Stars within spiral galaxies should rotate with a velocity depending on the radius to the galactic center, but **this is not what is observed experimentally** [3];
- Either our understanding of gravity at large scales or our basic understanding of galaxies as a celestial body made of stars has to be revised.



CMB anisotropies

- Background of primary radio waves emitted when the Universe became transparent around 380 000 years after the Big Bang;
- Can be considered as emitting a black body spectrum with a temperature of $(2.72548 \pm 0.00057)\text{K}$ [4], but small anisotropies at the 10^{-5} level are observed;
- Implies that dark matter **accounts for $\sim 27\%$ of the total mass of the Universe.**



Other observations, such as the gravitational lensing effect, **also tend to further support the existence of dark matter** (cf. backup).

Several fundamental properties of dark matter are nowadays known or assumed:

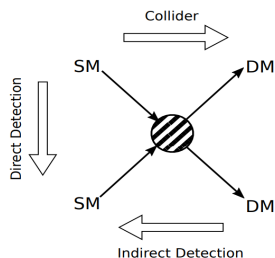
- Dark matter is a particle, given that it is assumed to have a certain mass;
- It should be dark, unable to interact with electromagnetic radiation, otherwise we would have seen it already. It should then also be electrically neutral;
- It is non-baryonic, because the energy density for the baryonic matter estimated from the CMB is too low to account for dark matter;
- We only consider cold dark matter since the widely accepted Λ_{CDM} model is based on this assumption and this helps explaining the presence of large scale structures in the Universe;
- It should have a mass in the electroweak scale, between 10 GeV and 1 TeV, because of the relic density obtained from the thermal freeze-out mechanism [5].
- Finally, it should be long-lived, since we expect them to have been produced during the Big Bang and they are still present in the Universe.

Weakly Interactive Massive Particles

The WIMPs are the dark matter candidates considered in this work, because of the so-called **WIMP miracle**. Indeed, they:

- Are expected to interact very weakly with ordinary baryonic matter;
- Have a mass in the 100 GeV-1 TeV range for reasonable electroweak production cross-section values;
- Give us a dark matter while being able to solve the **hierarchy problem**.

Main search strategies



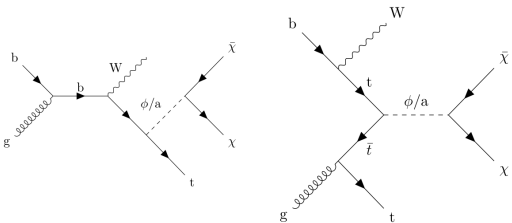
Different strategies are used:

- The **direct and indirect searches**, relying on the production of baryonic matter from the interaction between two DM particles or on the observation of the interaction between the dark and baryonic sectors;
- And the **collider production**, able to probe lower dark matter candidates masses.

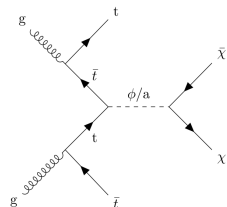
We are searching for **dark matter produced in association with either one or two top quarks**. Several **Simplified models** are considered:

- Spin 1/2 DM χ ($\in [1, 55]$ GeV, Dirac fermion)
- Spin 0 scalar (S)/pseudoscalar (PS) mediator ϕ (Yukawa-like structure of such interactions → gain from the coupling of the mediator to top quarks)
- Mediator mass $\in [10, 1000]$ GeV
- Coupling g_χ mediator/DM set to 1 (same for all g_q couplings)

$t/\bar{t}+\text{DM}$ tW models



$t\bar{t}+\text{DM}$ model



The **typical final state** of such models is made out of:

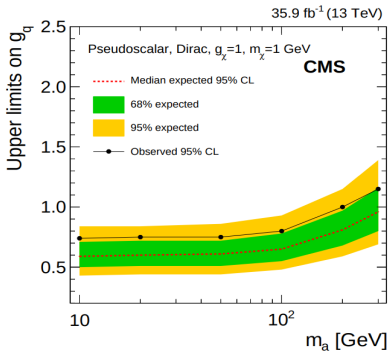
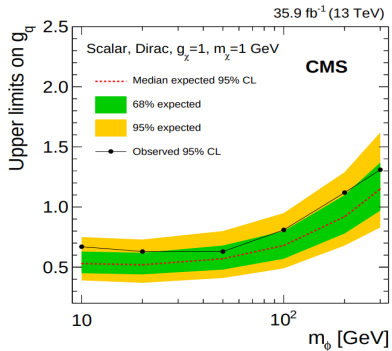
- 1 or 2 b-tagged jets coming from the decay of the top quark(s);
- 2 W bosons, seen as a combination of jets and leptons depending on the channel;
- Some MET coming from the dark matter and the decay of the Ws;

In particular, we are studying the **dilepton final state** in this work:

- Has the lowest branching ratio: $\text{BR}(W \rightarrow l^+ + \nu_l) = (10.80 \pm 0.09)\%$ for each of the three leptons (contains only 5% of the signal events);
- But, leptons can usually be reconstructed better than jets, resulting in lower systematic uncertainties;
- And this channel also has the lowest number of backgrounds, resulting in a better signal isolation.

This channel is then **expected to be competitive with the hadronic channel**, especially when considering high mediator masses, which feature a higher global discrimination signal/background.

A similar analysis has already been published by CMS using 2016 data, considering the $t\bar{t}+DM$ signal only and a combination of the three possible final states [7].



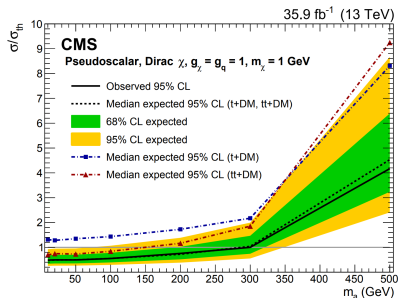
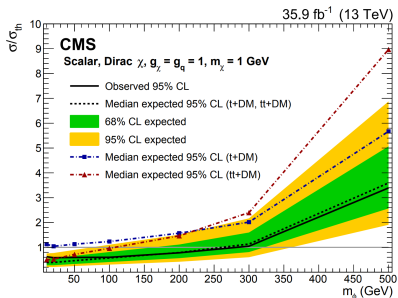
The observed (expected) limits excluded a **pseudoscalar mediator** with mass below 220 (320) GeV, and a **scalar mediator** with mass below 160 (240) GeV.

Previous relevant results II

A combination of both the t/\bar{t} +DM and $t\bar{t}$ +DM processes has also been performed.

The inclusion of the single top signal process improved up to a factor 2 the limits obtained by the $t\bar{t}$ analysis on its own [8]. This analysis:

- Only considered the 2016 data-taking period;
- And only considered the semi-leptonic and hadronic final states.



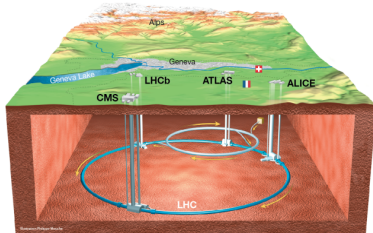
Scalar (pseudoscalar) mediators were with this combination excluded up to 290 (300) GeV at the 95% confidence level.

The experimental setup

The Large Hadron Collider I

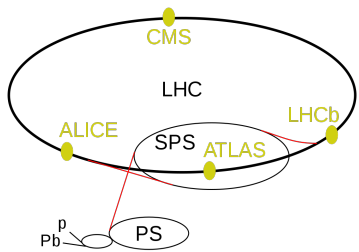
The data analyzed has been taken by the Large Hadron Collider:

- A 27km circular underground proton-proton collider, located at CERN;
- Result of the collaboration of 22 countries;
- Built in order to study and reproduce the conditions of the Universe at its origin;
- Provided the collisions that lead to the discovery of the Higgs boson in 2012 [9, 10];
- Currently the most powerful accelerator in the world with its center of mass energy $\sqrt{s} = 13$ TeV, therefore able to **scan new parts of the phase space**.



The data considered in this work has been collected during the **Run II of operation of the LHC** (from 2016 to 2018), at 13 TeV, totalling $(137.1 \pm 2.0) \text{ fb}^{-1}$ of data, selected by the different levels of trigger from the 40MHz collision rate.

In the 4 interaction points of the LHC, **4 detectors** have been placed: ATLAS, CMS, ALICE and LHCb, each having their own characteristics and features:



- ATLAS and CMS are **general purpose detectors**, able to study exotic processes such as well as able to make precision measurements on Standard Model physics;
- ALICE is mostly dedicated to the study of the quark-gluon plasma originating from heavy ions collisions;
- And LHCb has been designed to study the CP violation phenomena, which could be the sign of some new physics.

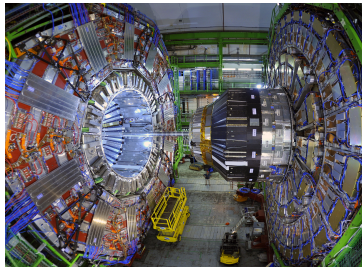
The collisions analyzed in this work **have been collected by the CMS detector**.

The **Compact Muon Solenoid** is one of the two general purpose detectors of the LHC. Its main objectives consist in:

- Searching for and studying the properties of the Higgs boson;
- Trying to discover new BSM physics, such as the possible existence of dark matter.

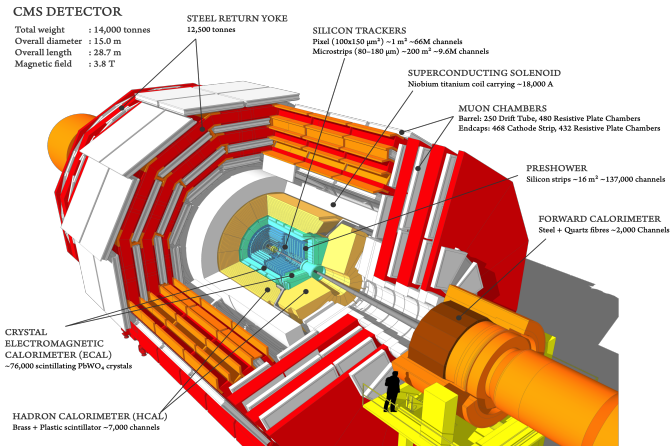
In a nutshell, CMS:

- Is a relatively **compact** (14.000 tons, distributed over a 15m diameter and a length of 8m) cylindrical detector;
- Is made out of a central part with cylindrical shape, the barrel, and two endcaps, one on each side in order to be **as hermetic as possible**, covering all the possible angles around the beam pipe;
- Has a **large solenoid** as middle piece, able to produce a 3.8T field;
- Features a **powerful tracker and muon detection system**.



The CMS detector II

The CMS detector is also **made out of different layers**, each having its own purpose, allowing for example to identify unequivocally each particle created.



Each subdetector of CMS has been designed carefully to fill its specific purpose:

- The **tracker** is the innermost piece of CMS, able to reconstruct the trajectories of charged particles issued from the interaction vertices in a quick and precise way;
- The **Electromagnetic CALorimeter**, enclosing the tracker system and able to give information about the energy of electrons and photons;
- The **Hadronic CALorimeter**, able to measure the energy of incident hadrons from the ionization process happening in its core;
- The 12.5 meters long and 6 meters large **solenoid**, allowing to measure precisely the charge and momentum of particles produced using the Lorentz effect, by measuring the curvature of their tracks;
- And finally, the **muon system**, covering more than $25\ 000\ m^2$ and made out of three different subsystems:
 - The **Drift Tubes** (DTs), in the barrel region;
 - The **Cathode Strip Chambers** (CSCs) in the two endcaps;
 - And the **Resistive Plate Chambers** (RPCs), mostly added to the barrel and to the endcap regions in order to cope with (in)ability of the previous muon system to identify unequivocally the correct bunch crossing when the LHC is running at full luminosity.

Global strategy

Run II legacy paper being worked on, expected to combine both the $t+DM$ and $t\bar{t}+DM$ searches, and the 3 possible final states (hadronic, semi-leptonic and dileptonic).

The effort is globally common between the groups:

- Objects will be defined in a common way
- Control and signal region orthogonal between the channels
 - Number of leptons and b-jet categorization to improve the sensitivity by defining enriched single top/ $t\bar{t}$ regions

Hadronic final state

Semi-leptonic final state

Dilepton final state

The main idea is to train a MVA (either BDT or DNN) to **separate the two signals from the backgrounds**, mainly the SM $t\bar{t}$ and the single top.

Frameworks

Two different frameworks used in coordination, by IFCA and DESY:

- Both using nanoAODv7 and the same background/signal samples;
- Synchronization exercise performed in the different control and signal regions, in 2016, 2017 and 2018, as documented in our twiki [11].

Data

Single/double leptons datasets built to avoid any eventual double counting, considering the 3 years of the Run II of operation of the LHC:

- $(35.9 \pm 0.9) \text{ fb}^{-1}$
- $(41.5 \pm 1.0) \text{ fb}^{-1}$
- $(59.7 \pm 1.5) \text{ fb}^{-1}$

A blinding policy is currently in place, allowing us to only look at 1 fb^{-1} of data per year near the signal regions.

Monte-Carlo

The major backgrounds have been considered from MC and read from NanoAOD:

- $t\bar{t}$: decaying to both 1 and 2 leptons;
- Single top: s, t and tW channels considered;
- Drell-Yan: HT-binned samples to increase the statistics, with a correction factor derived from data applied;
- TTZ and TTW: usually grouped together as TTV;
- Others: dibosons, tribosons, non-prompt contamination (data-driven, not MC).

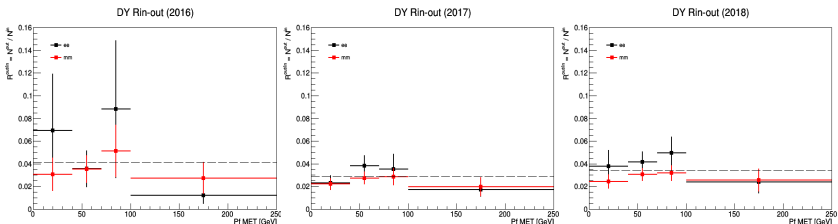
DY Rin-out method

We want to estimate the DY yields outside of the Z-peak from the data:

- Given the presence of large backgrounds (such as $t\bar{t}$) in the analysis region, we go inside of the Z-peak to compute the **Rin-out factor**:

$$N_{DY}^{out} = N_{DY, data}^{in} \cdot \left(\frac{N_{DY, MC}^{out}}{N_{DY, MC}^{in}} \right) \equiv N_{DY, data}^{in} \cdot R_{out/in, MC}$$

- To avoid any bias, the contamination of non-peaking backgrounds is removed and we additionally correct this factor by the ratio between the data/MC transfer factors in a CR close to the SR (asking for 0 b-jet instead of 1);
- We then get this Rin-out in bins of MET and for each channel (ee , $\mu\mu$) separately:



A flat scale factor and a fixed 20% systematic uncertainty is then applied to the DY.

Non-prompt contamination I

Fake leptons detection in the detector needs to be taken into account properly, through a **data-driven tight-to-loose method** since the Monte-Carlo is not reliable in this case:

Fake rate

- A QCD enriched region is defined with a looser particle selection criteria, where the misidentification should be high;
- Any eventual contamination from electroweak processes in this region is removed;
- The **fake rate** is defined as the ratio between the fakeable object (lepton-like objects passing only the loose isolation requirements) and fully selected objects yields.

Prompt rate

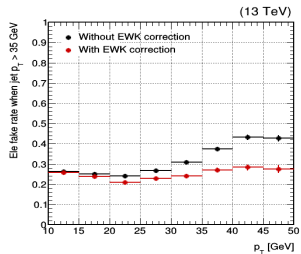
- The **prompt rate**, taking into account the real lepton contamination is calculated in a Z enriched region from a general tag and probe method.

Then, we calculate from data an extrapolation factor to go back to the signal region of the analysis and the results obtained are checked in a **same sign control region**.

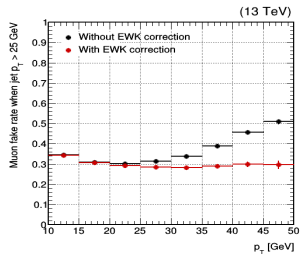
Non-prompt contamination II

2016 fake rate

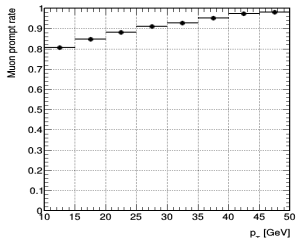
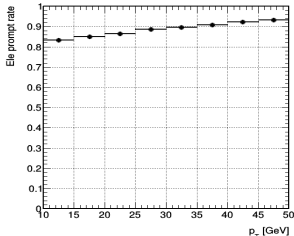
Electron



Muon

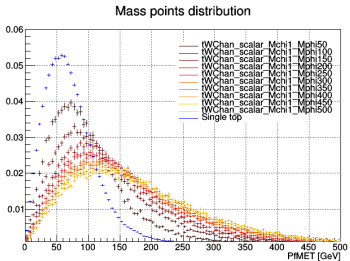


2016 prompt rate

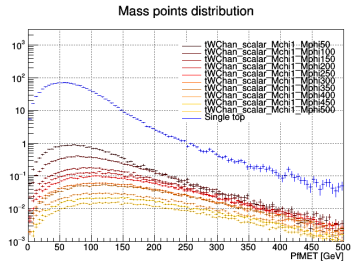


Scalar mediators

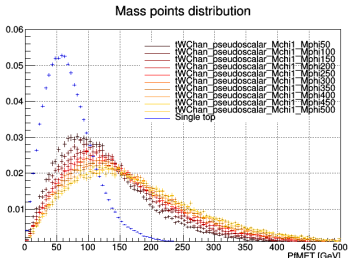
With normalization



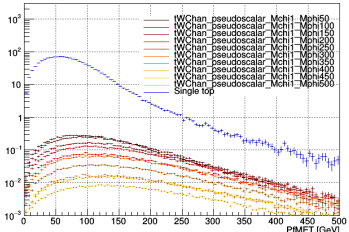
Without normalization



Pseudoscalar mediators

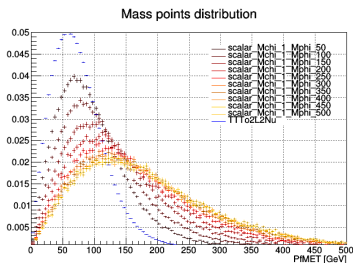


Mass points distribution

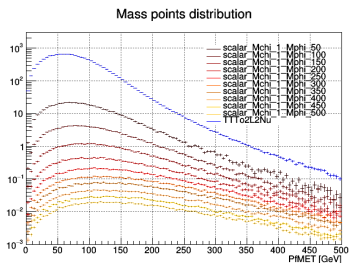


Scalar mediators

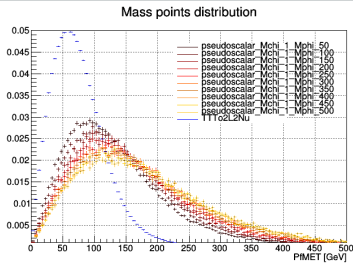
With normalization



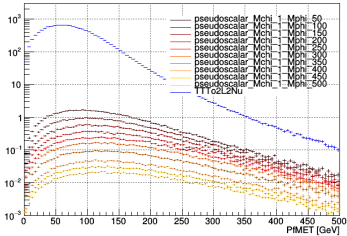
Without normalization



Pseudoscalar mediators



Mass points distribution



Objects definition

Control regions

- An **inclusive** region:
 - Exactly 2 tight leptons ($p_T > 25, 20$ GeV)
 - Opposite sign leptons
 - $m_{ll} > 20$ GeV
 - At least 1 jet ($p_T > 30$ GeV, $|\eta| < 2.4$)
 - At least 1 deep CSV b-jet (medium WP)
- A **Drell-Yan CR**, defined as the inclusive region and:
 - 15 GeV Z window ($ee/\mu\mu$ channels)
 - $m_{T2}^H > 80$ GeV
- A **$t\bar{t}$** CR, similar to the $t\bar{t} + \text{DM}$ signal region:
 - But only for events classified as background by the MVA
 - Currently blinded to 1fb^{-1} per year
- A **ttV** ($ttW + ttZ$) CR:
 - At least 3 tight leptons
 - $m_{T2}^H > 80$ GeV
- A **same-sign CR** for the non-prompt background:
 - Inclusive with same sign leptons
 - 15 GeV Z-veto ($ee/\mu\mu$ channels)

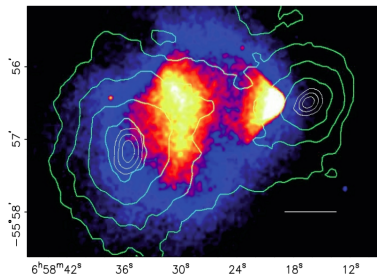
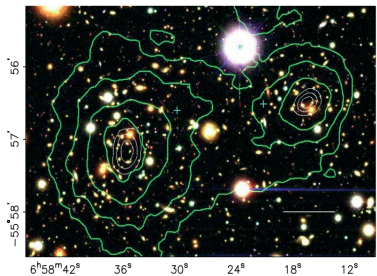
Conclusions

Back up

Gravitational lensing

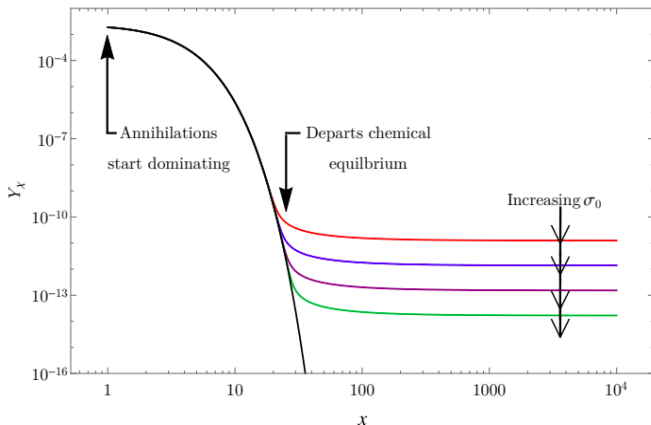
Consequence of the general relativity: massive objects placed between distant sources and the observer should be able to act as lenses and bend the light of the source.

- The deviation of the light is proportional to the mass of the intermediate object, giving us a way to measure its mass;
- The mass distribution obtained has been compared to the luminous distribution of several galaxies, leading to 8σ discrepancies [6].



Thermal freeze-out

Schematic representation of the freeze-out process, representing the abundance of a 500 GeV dark matter with respect to the time and the impact of increasing cross-section annihilation values on this freeze-out abundance.



Center of mass energy

The center of mass energy is defined as a Lorentz invariant quantity under any kind of boost resulting of the collisions between two protons (defined as E_1, \vec{p}_1, m_1 and E_2, \vec{p}_2, m_2) with a θ angle.

$$\sqrt{s} = \sqrt{(m_1)^2 + (m_2)^2 + 2(E_1 E_2 - 2|\vec{p}_1| |\vec{p}_2| \cos(\theta))}$$

The LHC started its operation in 2008 running at an energy of 7 TeV, quickly moved to 8 TeV and kept this level of energy during the end of the Run I of operation. In 2015, the energy was increased to 13 TeV.

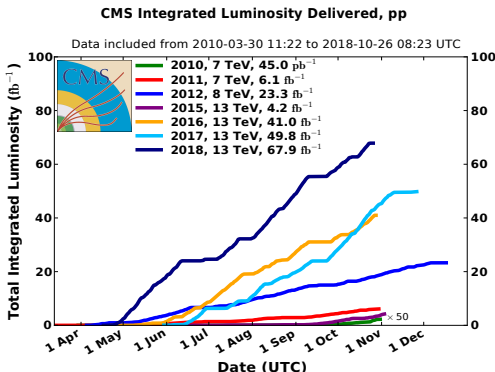
An expected value of 14 TeV, the nominal energy for which the LHC was originally built, is expected to be reached in the near future.

Luminosity

The luminosity gives an indication on the number of collisions per second given by the accelerator. Increasing it is crucial to collect as much data as possible, to be able to isolate processes having a low production cross section.

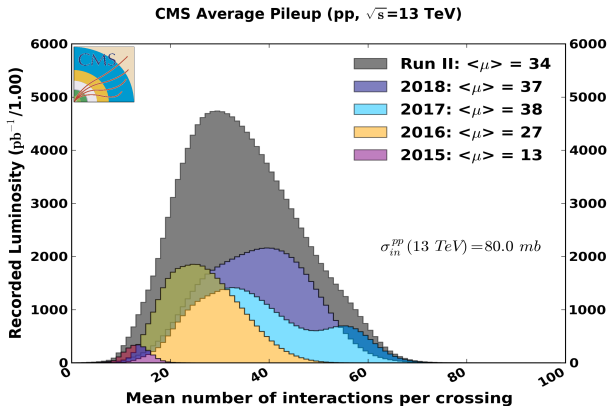
The rate of production R of any given process can be expressed from the instantaneous luminosity $\mathcal{L}(t)$ and the process production cross-section σ :

$$\begin{cases} R = \mathcal{L} \cdot \sigma \\ N(T) = \sigma \int_0^T \mathcal{L}(t) dt = \sigma L \end{cases}$$



Pile-up

Because of the high density of protons within the beams, a bunch crossing in an experiment produces around 30-35 proton collisions.



The Primary Vertex is defined as the most interesting and energetic vertex, while the other vertices are usually referred to as the pile-up.

LHC operational parameters

Key parameters of operation of the LHC, depending on the data-taking period:

Parameter	Run I	Run II	Run III	Design
Energy [TeV]	7 → 8	13	13	14
Bunch spacing [ns]	50	25	25	25
Intensity [10^{11} protons per beam]	1.6	1.2	Up to 1.8	1.15
Bunches	1400	2500	2800	2800
Emittance [μm]	2.2	2.2	2.5	3.5
β^* [cm]	80	30 → 25	30 → 25	55
Crossing angle [μrad]	-	300 → 260	300 → 260	285
Peak luminosity [$10^{34} \text{ cm}^{-2} \text{ s}^{-1}$]	0.8	2.0	2.0	1.0
Peak pile-up	45	60	55	25

The tracker is the innermost piece of CMS, able to reconstruct the trajectories of charged particles issued from the interaction vertices in a quick and precise way:

- Needs to be extremely fast to read the 40MHz of collision data, while being resistant to the radiation (expected lifetime ~ 10 years);
- It should be as small as possible to minimize the interaction between the detector and the particles created;
- However, fast electronics usually needs to be cooled down, which increases the size of the subdetector.

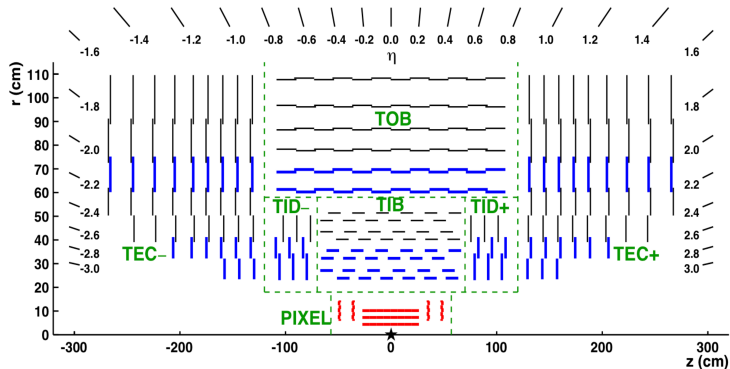
Made out of two main parts:

- The **pixel detector**, made out 60 millions pixels which make up the 1856 active modules of this detector, covering an area of $\sim 1 \text{ m}^2$;
- The **silicon strip detector**, covering an area of $\sim 200 \text{ m}^2$, and made out of three different sub-systems for hermeticity.

A charged particle crossing the tracker will leave a hit each time it crosses one of the silicon sensors, allowing us to reconstruct its track.

The silicon detector is divided into three main parts:

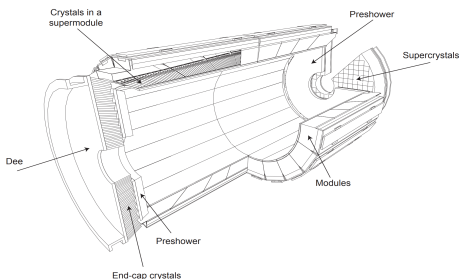
- The Tracker Inner Barrel and Disks (TIB/TBD), using micro-strips parallel in the barrel and perpendicular to the beam axis in the endcaps;
- The Tracker Outer Barrel (TOB), adding 6 measurement layers to the tracker;
- And finally the Tracker EndCaps (TECs), made out of 9 disks, completing the system at high pseudorapidities.



The ECAL is a subdetector sitting inside the solenoid but enclosing the tracker system that gives information about the energy of electrons and photons, both able to interact electromagnetically with its crystals.

Made out of different layers:

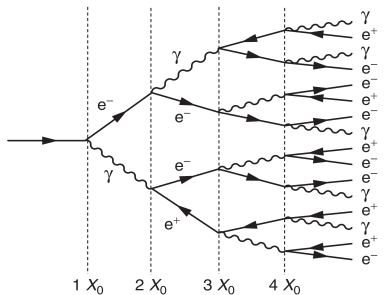
- The barrel part (EB), at $|\eta| < 1.479$, made out of 61 200 lead tungstate (PbWO_4) crystals;
- Two endcaps, each made out of 7 324 crystals, increasing the coverage of the detector up to $|\eta| < 3$;
- The preshower, helping with the identification of electrons against minimum ionizing particles.



The principle of action of the ECAL is simple, and is based on **electromagnetic showers**. When an electron or a photon enters the ECAL, it starts to interact in different ways:

- Photons will mainly produce pairs of electrons and anti-electrons;
- Electrons themselves tend to emit additional photons by bremsstrahlung effect.

This results in a chain reaction during which the incident particle gives most of its energy to the detector, energy measurable using photodetectors and photomultipliers.



Although quite fragile and sensitive to the temperature, the short radiation length X_0 of the $PbWO_4$ crystals is an advantage, along with their scintillation decay time smaller than the bunch crossing.

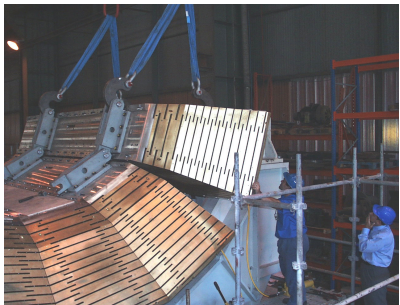
Each crystal measures $2.2 \times 2.2 \times 23$ cm, corresponding to 26 radiation lengths.

Charged hadrons lose energy when they traverse matter due to the ionization process resulting from the strong interaction between them and the nuclei of the detector.

Showers of particles are typically produced since the primary hadronic interaction will produce several additional hadrons, themselves interacting even more with the detector.

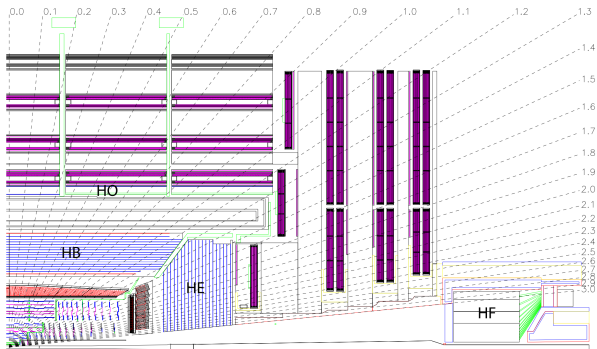
The HCAL is made out of alternating layers:

- Of thick **absorber material**, in which the showers can develop;
- And thin layers of **active material** used for the actual detection by sampling the energy deposition.



The HCAL is divided into:

- A barrel (HB), up to $|\eta| = 1.3$;
- Two endcaps, extending the pseudorapidities coverage up to $|\eta| = 3.0$;
- Two symmetrical forward regions (HF), covering up to $|\eta| = 5.2$;
- And the Hadron Outer (HO), outside of the solenoid, placed to increase the effective nuclear radiation length λ , otherwise low at a 90° incidence angle.



CMS solenoid

The superconducting solenoid:

- Is made out of 6 endcap disks and 5 barrel wheels;
- Weights more than 12 000 tons in total, with the return yoke;
- Is able to produce a 3.8T magnetic field once cooled down to 4.5K;
- Stores at all times around 2.6GJ of energy.



It allows the measurement of the momentum and charge of particles by studying the curvature of their tracks, according to the Lorentz equation:

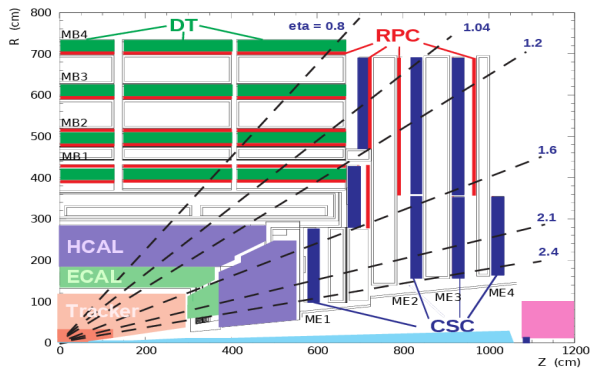
$$\vec{F} = \frac{m\vec{v}^2}{R} = q\vec{E} + q\vec{v} \times \vec{B} = q\vec{v} \times \vec{B}$$

It has been designed to reach a momentum resolution $\Delta p/p \sim 10\%$ at $p = 1$ TeV.

CMS muon systems I

The muon systems is the outermost section of CMS, covering around 25 000 m².

Three different categories of devices have been designed, in order to cope with the specific experimental conditions in the different parts of the detector: the Drift Tubes (DTs), the Cathode Strips Chambers (CSCs), and the Resistive Plate Chambers (RPCs).



All these detectors are gaseous, distributed over a cylindrical area given the shape of the innermost components of CMS, and cheap, given the large surface they cover.

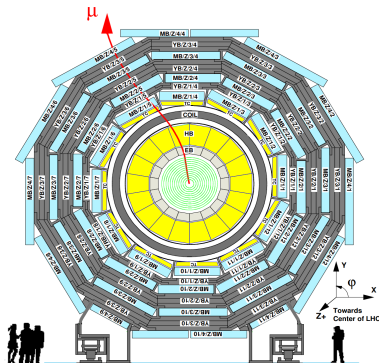
Comparison of the different subsystems:

Muon sub-system	DTs	CSCs	RPCs
$ \eta $ coverage Stations	0.0-1.2 4	0.9-2.4 4	0.0-1.9 4
Chambers	250	540	480 (barrel) 576 (endcaps)
Readout channels	172 000	266 112 (strips) 210 816 (anode channels)	68 136 (barrel) 55 296 (endcaps)
Spatial resolution	80-120 μm	40-150 μm	0.8-1.2 cm
Average efficiency (13 TeV)	97.1%	97.4%	94.2% (barrel) 96.4% (endcaps)

Placed in the barrel region (up to $|\eta| = 1.2$), where the background levels and magnetic field are low, this system allows a good efficiency for the muon hits reconstruction into a single track and a good rejection of eventual background hits.

This system is:

- Able to collect the residuals charges left by the ionization tracks of muons;
- Made out of 172 000 sensitive wires, divided in 250 chambers;
- Redundant, by the installation of 4 layers, to reduce the impact coming from eventual neutrons or photons;
- Has a maximal drift time of 380ns, low enough to avoid the need of multi-hits electronics.



2016 data samples

Dataset	Events (size)	\mathcal{L} [fb^{-1}]
Run 2016B		
/DoubleEG/Run2016B_ver2-Nano02Apr2020_ver2-v1/NANOAOOD	143073268 (99.4Gb)	
/DoubleMuon/Run2016B_ver2-Nano02Apr2020_ver2-v1/NANOAOOD	82535526 (53.2Gb)	
/MuonEG/Run2016B_ver2-Nano02Apr2020_ver2-v1/NANOAOOD	32727796 (26.8Gb)	5.8
/SingleElectron/Run2016B_ver2-Nano02Apr2020_ver2-v1/NANOAOOD	246440440 (167.8Gb)	
/SingleMuon/Run2016B_ver2-Nano02Apr2020_ver2-v1/NANOAOOD	158145722 (96.4Gb)	
Run 2016C		
/DoubleEG/Run2016C-Nano02Apr2020-v1/NANOAOOD	47677856 (35.3Gb)	
/DoubleMuon/Run2016C-Nano02Apr2020-v1/NANOAOOD	27934629 (19.7Gb)	
/MuonEG/Run2016C-Nano02Apr2020-v1/NANOAOOD	15405678 (12.8Gb)	2.6
/SingleElectron/Run2016C-Nano02Apr2020-v1/NANOAOOD	97259854 (69.3Gb)	
/SingleMuon/Run2016C-Nano02Apr2020-v1/NANOAOOD	67441308 (42.4Gb)	
Run 2016D		
/DoubleEG/Run2016D-Nano02Apr2020-v1/NANOAOOD	53324960 (39.6Gb)	
/DoubleMuon/Run2016D-Nano02Apr2020-v1/NANOAOOD	33861745 (24.1Gb)	
/MuonEG/Run2016D-Nano02Apr2020-v1/NANOAOOD	23482352 (19.4Gb)	4.2
/SingleElectron/Run2016D-Nano02Apr2020-v1/NANOAOOD	148167727 (104.4Gb)	
/SingleMuon/Run2016D-Nano02Apr2020-v1/NANOAOOD	98017996 (61.3Gb)	
Run 2016E		
/DoubleEG/Run2016E-Nano02Apr2020-v1/NANOAOOD	49877710 (37.9Gb)	
/DoubleMuon/Run2016E-Nano02Apr2020-v1/NANOAOOD	28246946 (20.8Gb)	
/MuonEG/Run2016E-Nano02Apr2020-v2/NANOAOOD	22519303 (19.0Gb)	4.0
/SingleElectron/Run2016E-Nano02Apr2020-v1/NANOAOOD	117321545 (86.5Gb)	
/SingleMuon/Run2016E-Nano02Apr2020-v1/NANOAOOD	90984718 (58.7Gb)	
Run 2016F		
/DoubleEG/Run2016F-Nano02Apr2020-v1/NANOAOOD	34577629 (26.9Gb)	
/DoubleMuon/Run2016F-Nano02Apr2020-v1/NANOAOOD	20329921 (15.3Gb)	
/MuonEG/Run2016F-Nano02Apr2020-v1/NANOAOOD	16002165 (13.6Gb)	3.1
/SingleElectron/Run2016F-Nano02Apr2020-v1/NANOAOOD	70593532 (51.4Gb)	
/SingleMuon/Run2016F-Nano02Apr2020-v1/NANOAOOD	65489554 (42.4Gb)	
Run 2016G		
/DoubleEG/Run2016G-Nano02Apr2020-v1/NANOAOOD	78797031 (61.6Gb)	
/DoubleMuon/Run2016G-Nano02Apr2020-v1/NANOAOOD	45235604 (34.2Gb)	
/MuonEG/Run2016G-Nano02Apr2020-v1/NANOAOOD	33854612 (29.0Gb)	7.6
/SingleElectron/Run2016G-Nano02Apr2020-v1/NANOAOOD	153363109 (109.2Gb)	
/SingleMuon/Run2016G-Nano02Apr2020-v1/NANOAOOD	149912248 (94.6Gb)	
Run 2016H		
/DoubleEG/Run2016H-Nano02Apr2020-v1/NANOAOOD	85388734 (67.7Gb)	
/DoubleMuon/Run2016H-Nano02Apr2020-v1/NANOAOOD	48912812 (37.3Gb)	
/MuonEG/Run2016H-Nano02Apr2020-v1/NANOAOOD	29236516 (26.0Gb)	8.6
/SingleElectron/Run2016H-Nano02Apr2020-v1/NANOAOOD	128854598 (93.8Gb)	
/SingleMuon/Run2016H-Nano02Apr2020-v1/NANOAOOD	174035164 (110.2Gb)	

2017 data samples

Dataset	Events (size)	\mathcal{L} [fb $^{-1}$]
Run 2017B		
/DoubleEG/Run2017B-Nano02Apr2020-v1/NANOAOD	58088760 (46.6Gb)	
/DoubleMuon/Run2017B-Nano02Apr2020-v1/NANOAOD	14501767 (10.8Gb)	
/SingleElectron/Run2017B-Nano02Apr2020-v1/NANOAOD	60537490 (42.2Gb)	
/SingleMuon/Run2017B-Nano02Apr2020-v1/NANOAOD	136300266 (86.2Gb)	
/MuonEG/Run2017B-Nano02Apr2020-v1/NANOAOD	4453465 (4.1Gb)	
Run 2017C		
/DoubleEG/Run2017C-Nano02Apr2020-v1/NANOAOD	65181125 (53.8Gb)	
/DoubleMuon/Run2017C-Nano02Apr2020-v1/NANOAOD	49636525 (39.5Gb)	
/SingleElectron/Run2017C-Nano02Apr2020-v1/NANOAOD	136637888 (102.5Gb)	
/SingleMuon/Run2017C-Nano02Apr2020-v1/NANOAOD	165652756 (109.5Gb)	
/MuonEG/Run2017C-Nano02Apr2020-v1/NANOAOD	15595214 (15.0Gb)	
Run 2017D		
/DoubleEG/Run2017D-Nano02Apr2020-v1/NANOAOD	25911432 (21.6Gb)	
/DoubleMuon/Run2017D-Nano02Apr2020-v1/NANOAOD	23075733 (18.6Gb)	
/SingleElectron/Run2017D-Nano02Apr2020-v1/NANOAOD	51526710 (38.5Gb)	
/SingleMuon/Run2017D-Nano02Apr2020-v1/NANOAOD	70361660 (47.2Gb)	
/MuonEG/Run2017D-Nano02Apr2020-v1/NANOAOD	9164365 (8.9Gb)	
Run 2017E		
/DoubleEG/Run2017E-Nano02Apr2020-v1/NANOAOD	56233597 (49.8Gb)	
/DoubleMuon/Run2017E-Nano02Apr2020-v1/NANOAOD	51589091 (44.4Gb)	
/SingleElectron/Run2017E-Nano02Apr2020-v1/NANOAOD	102121689 (81.3Gb)	
/SingleMuon/Run2017E-Nano02Apr2020-v1/NANOAOD	154630534 (111.0Gb)	
/MuonEG/Run2017E-Nano02Apr2020-v1/NANOAOD	19043421 (19.2Gb)	
Run 2017F		
/DoubleEG/Run2017F-Nano02Apr2020-v1/NANOAOD	74307066 (67.1Gb)	
/DoubleMuon/Run2017F-Nano02Apr2020-v1/NANOAOD	79756560 (68.0Gb)	
/SingleElectron/Run2017F-Nano02Apr2020-v1/NANOAOD	128467223 (105.2Gb)	
/SingleMuon/Run2017F-Nano02Apr2020-v1/NANOAOD	242135500 (178.3Gb)	
/MuonEG/Run2017F-Nano02Apr2020-v1/NANOAOD	25776363 (26.3Gb)	

2018 data samples

Dataset	Events (size)	\mathcal{L} [fb^{-1}]
Run 2018A		
/DoubleMuon/Run2018A-Nano02Apr2020-v1/NANO AOD	75499908 (62.6Gb)	
/EGamma/Run2018A-Nano02Apr2020-v1/NANO AOD	327843843 (261.8Gb)	
/SingleMuon/Run2018A-Nano02Apr2020-v1/NANO AOD	241608232 (167.7Gb)	13.5
/MuonEG/Run2018A-Nano02Apr2020-v1/NANO AOD	32958503 (32.3Gb)	
Run 2018B		
/DoubleMuon/Run2018B-Nano02Apr2020-v1/NANO AOD	35057758 (28.3Gb)	
/EGamma/Run2018B-Nano02Apr2020-v1/NANO AOD	153822427 (123.1Gb)	
/SingleMuon/Run2018B-Nano02Apr2020-v1/NANO AOD	119918017 (82.3Gb)	6.8
/MuonEG/Run2018B-Nano02Apr2020-v1/NANO AOD	16211567 (15.8Gb)	
Run 2018C		
/DoubleMuon/Run2018C-Nano02Apr2020-v1/NANO AOD	34565869 (27.6Gb)	
/EGamma/Run2018C-Nano02Apr2020-v1/NANO AOD	147827904 (119.2Gb)	
/SingleMuon/Run2018C-Nano02Apr2020-v1/NANO AOD	110032072 (75.7Gb)	6.6
/MuonEG/Run2018C-Nano02Apr2020-v1/NANO AOD	15652198 (15.3Gb)	
Run 2018D		
/DoubleMuon/Run2018D-Nano02Apr2020_ver2-v1/NANO AOD	168605834 (128.6Gb)	
/EGamma/Run2018D-Nano02Apr2020-v1/NANO AOD	751348648 (583.6Gb)	
/SingleMuon/Run2018D-Nano02Apr2020-v1/NANO AOD	513867253 (344.5Gb)	
/MuonEG/Run2018D-Nano02Apr2020_ver2-v1/NANO AOD	71961587 (68.6Gb)	32.0

2016 MC samples

Process	Sample	Cross section [pb]
Drell-Yan	DYJetsToLL_M-10to50_TuneCUETP8M1_13TeV-madgraphMLM-pythia8 ($H_T < 70$ GeV) DYJetsToLL_M-5to50_HT-70to100_TuneCUETP8M1_13TeV-madgraphMLM-pythia8 DYJetsToLL_M-5to50_HT-100to200_TuneCUETP8M1_13TeV-madgraphMLM-pythia8 DYJetsToLL_M-5to50_HT-200to400_TuneCUETP8M1_13TeV-madgraphMLM-pythia8 DYJetsToLL_M-5to50_HT-400to600_TuneCUETP8M1_13TeV-madgraphMLM-pythia8 DYJetsToLL_M-5to50_HT-600toInf_TuneCUETP8M1_13TeV-madgraphMLM-pythia8 DYJetsToLL_M-50_TuneCUETP8M1_13TeV-madgraphMLM-pythia8 ($H_T < 70$ GeV) DYJetsToLL_M-50_HT-70to100_TuneCUETP8M1_13TeV-madgraphMLM-pythia8 DYJetsToLL_M-50_HT-100to200_TuneCUETP8M1_13TeV-madgraphMLM-pythia8 DYJetsToLL_M-50_HT-200to400_TuneCUETP8M1_13TeV-madgraphMLM-pythia8 DYJetsToLL_M-50_HT-400to600_TuneCUETP8M1_13TeV-madgraphMLM-pythia8 DYJetsToLL_M-50_HT-600to800_TuneCUETP8M1_13TeV-madgraphMLM-pythia8 DYJetsToLL_M-50_HT-800to1200_TuneCUETP8M1_13TeV-madgraphMLM-pythia8 DYJetsToLL_M-50_HT-1200to2500_TuneCUETP8M1_13TeV-madgraphMLM-pythia8 DYJetsToLL_M-50_HT-2500toInf_TuneCUETP8M1_13TeV-madgraphMLM-pythia8	18610.0 303.8 224.2 37.2 3.581 1.124 6025.20 169.9 147.4 40.99 5.678 1.367 0.6304 0.1514 0.003565
TTTo2L2Nu	TTTo2L2Nu_TuneCUETP8M2_ttHtranche3_13TeV-powheg-pythia8	87.310
Single top	ST_s-channel_4f_leptonDecays_13TeV-amcatnlo-pythia8_TuneCUETP8M1 ST_t-channel_antitop_4f_inclusiveDecays_13TeV-powhegV2-madspin-pythia8_TuneCUETP8M1 ST_t-channel_top_4f_inclusiveDecays_13TeV-powhegV2-madspin-pythia8_TuneCUETP8M1 ST_tW_antitop_5f_inclusiveDecays_13TeV-powheg-pythia8_TuneCUETP8M1 ST_tW_top_5f_inclusiveDecays_13TeV-powheg-pythia8_TuneCUETP8M1	3.360 80.95 136.02 35.60 35.60
WW	WWTo2L2Nu_13TeV-powheg WWJJToLNuLNu_EWK_noTop_13TeV-madgraph-pythia8 GluGluWWTo2L2Nu_MCFM_13TeV	12.178 0.34520 0.5905
V γ /V γ^*	WGToLNuG_TuneCUETP8M1_13TeV-madgraphMLM-pythia8 ZGTo2LG_TuneCUETP8M1_13TeV-amcatnloFXFX-pythia8 WZTo3LNu_mlmin01_13TeV-powheg-pythia8	405.271 131.300 58.59
VZ	ZZTo2L2Nu_13TeV-powheg_pythia8 ZZTo2L2Q_13TeV-powheg_pythia8 ZZTo4L_TuneCP5_13TeV_powheg_pythia8 WZTo2L2Q_13TeV_amcatnloFXFX_madspin_pythia8	0.5640 3.22 1.212 5.595
VVV	ZZZ_TuneCUETP8M1_13TeV-amcatnlo-pythia8 WZZ_TuneCUETP8M1_13TeV-amcatnlo-pythia8 WWZ_TuneCUETP8M1_13TeV-amcatnlo-pythia8 WWW_4F_TuneCUETP8M1_13TeV-amcatnlo-pythia8	0.01398 0.05565 0.16510 0.18331
Non-Prompt	Data-driven (tight-to-loose method)	

2017 MC samples

Process	Sample	Cross section [pb]
Drell-Yan	DYJetsToLL_M-10to50_TuneCP5_13TeV-madgraphMLM-pythia8 ($H_T < 100$ GeV)	18610
	DYJetsToLL_M-4to50_HT-100to200_TuneCP5_13TeV-madgraphMLM-pythia8	204.0
	DYJetsToLL_M-4to50_HT-200to400_TuneCP5_13TeV-madgraphMLM-pythia8	54.39
	DYJetsToLL_M-4to50_HT-400to600_TuneCP5_13TeV-madgraphMLM-pythia8	5.697
	DYJetsToLL_M-4to50_HT-600toInf_TuneCP5_13TeV-madgraphMLM-pythia8	1.85
	DYJetsToLL_M-50_TuneCP5_13TeV-madgraphMLM-pythia8 ($H_T < 70$ GeV)	6189.39
	DYJetsToLL_M-50_HT-70to100_TuneCP5_13TeV-madgraphMLM-pythia8	169.9
	DYJetsToLL_M-50_HT-100to200_TuneCP5_13TeV-madgraphMLM-pythia8	161.1
	DYJetsToLL_M-50_HT-200to400_TuneCP5_13TeV-madgraphMLM-pythia8	48.66
	DYJetsToLL_M-50_HT-400to600_TuneCP5_13TeV-madgraphMLM-pythia8	6.968
	DYJetsToLL_M-50_HT-600to800_TuneCP5_13TeV-madgraphMLM-pythia8	1.743
	DYJetsToLL_M-50_HT-800to1200_TuneCP5_13TeV-madgraphMLM-pythia8	0.8052
	DYJetsToLL_M-50_HT-1200to2500_TuneCP5_13TeV-madgraphMLM-pythia8	0.1933
	DYJetsToLL_M-50_HT-2500toInf_TuneCP5_13TeV-madgraphMLM-pythia8	0.003468
TTTo2L2Nu	TTTo2L2Nu_TuneCP5_13TeV-powheg-pythia8	87.310
Single top	ST_s-channel_4f_leptonDecays_mtop1715_TuneCP5_PSweights_13TeV-amcatnlo-pythia8	3.360
	ST_t-channel_antitop_4f_inclusiveDecays_TuneCP5_13TeV-powhegV2-madspin-pythia8	80.95
	ST_t-channel_top_4f_inclusiveDecays_TuneCP5_13TeV-powhegV2-madspin-pythia8	136.02
	ST_tW_antitop_5f_inclusiveDecays_TuneCP5_13TeV-powheg-pythia8	35.60
	ST_tW_top_5f_inclusiveDecays_TuneCP5_13TeV-powheg-pythia8	35.60
WW	WWTo2L2Nu_NNPDF31_TuneCP5_PSweights_13TeV-powheg-pythia8	12.178
	WWJJToLNuLNu_EWK_noTop_TuneCP5_13TeV-madgraph-pythia8	0.34520
	GluGluToWWTo*_13TeV_MCFM701_pythia8	0.06387
$V\gamma/V\gamma^*$	WGToLNuG_TuneCP5_13TeV-madgraphMLM-pythia8	405.271
	ZGToLLG_01J_5f_TuneCP5_13TeV-amcatnloFXFX-pythia8	58.83
	WZTo3LNu_mllmin01_NNPDF31_TuneCP5_13TeV_powheg_pythia8	58.59
VZ	ZZTo2L2Nu_13TeV_powheg_pythia8	0.5640
	ZZTo2L2Q_13TeV_amcatnloFXFX_madspin_pythia8	3.22
	ZZTo4L_TuneCP5_13TeV_powheg_pythia8	1.212
	WZTo2L2Q_13TeV_amcatnloFXFX_madspin_pythia8	5.595
VVV	ZZZ_TuneCP5_13TeV-amcatnlo-pythia8	0.01398
	WZZ_TuneCP5_13TeV-amcatnlo-pythia8	0.05565
	WWZ_4F_TuneCP5_13TeV-amcatnlo-pythia8	0.16510
	WWW_4F_TuneCP5_13TeV-amcatnlo-pythia8	0.18331
Non-Prompt	Data-driven (tight-to-loose method)	

2018 MC samples

Process	Sample	Cross section [pb]
Drell-Yan	DYJetsToLL_M-10to50_TuneCP5_13TeV-madgraphMLM-pythia8 ($H_T < 100$ GeV)	18610.0
	DYJetsToLL_M-4to50_HT-100to200_TuneCP5_PSweights_13TeV-madgraphMLM-pythia8	204.0
	DYJetsToLL_M-4to50_HT-200to400_TuneCP5_PSweights_13TeV-madgraphMLM-pythia8	54.39
	DYJetsToLL_M-4to50_HT-400to600_TuneCP5_PSweights_13TeV-madgraphMLM-pythia8	5.697
	DYJetsToLL_M-4to50_HT-600toInf_TuneCP5_PSWeights_13TeV-madgraphMLM-pythia8	1.85
	DYJetsToLL_M-50_TuneCP5_13TeV-amcatnloFXFX-pythia8 ($H_T < 70$ GeV)	6189.39
	DYJetsToLL_M-50_HT-70to100_TuneCP5_PSweights_13TeV-madgraphMLM-pythia8	169.9
	DYJetsToLL_M-50_HT-100to200_TuneCP5_PSweights_13TeV-madgraphMLM-pythia8	161.1
	DYJetsToLL_M-50_HT-200to400_TuneCP5_PSweights_13TeV-madgraphMLM-pythia8	48.66
	DYJetsToLL_M-50_HT-400to600_TuneCP5_PSweights_13TeV-madgraphMLM-pythia8	6.968
	DYJetsToLL_M-50_HT-600to800_TuneCP5_PSweights_13TeV-madgraphMLM-pythia8	1.743
	DYJetsToLL_M-50_HT-800to1200_TuneCP5_PSweights_13TeV-madgraphMLM-pythia8	0.8052
	DYJetsToLL_M-50_HT-1200to2500_TuneCP5_PSweights_13TeV-madgraphMLM-pythia8	0.1933
	DYJetsToLL_M-50_HT-2500toInf_TuneCP5_PSweights_13TeV-madgraphMLM-pythia8	0.003468
TTTo2L2Nu	TTTo2L2Nu_TuneCP5_13TeV-powheg-pythia8	87.310
Single top	ST_s-channel_4f_leptonDecays_TuneCP5_13TeV-madgraph-pythia8	3.360
	ST_t-channel_antitop_4f_InclusiveDecays_TuneCP5_13TeV-powheg-madspin-pythia8	80.95
	ST_t-channel_top_4f_InclusiveDecays_TuneCP5_13TeV-powheg-madspin-pythia8	136.02
	ST_tW_antitop_5f_inclusiveDecays_TuneCP5_13TeV-powheg-pythia8	35.60
	ST_tW_top_5f_inclusiveDecays_TuneCP5_13TeV-powheg-pythia8	35.60
WW	WWTo2L2Nu_NNPDF31_TuneCP5_13TeV-powheg-pythia8	12.178
	WWJToLNuLNu_EWK_TuneCP5_13TeV-madgraph-pythia8	0.4286
	GluGluToWWTo*_TuneCP5_13TeV_MCFM701_pythia8	0.06387
V γ /V γ^*	WGToLNuG_TuneCP5_13TeV-madgraphMLM-pythia8	405.271
	ZGToLLG_0J1_5f_TuneCP5_13TeV-amcatnloFXFX-pythia8	131.300
	WZTo3LNu_mlmin01_NNPDF31_TuneCP5_13TeV_powheg_pythia8	58.59
VZ	ZZTo2L2Nu_TuneCP5_13TeV_powheg_pythia8	0.5640
	ZZTo2L2Q_13TeV_amcatnloFXFX_madspin_pythia8	3.22
	ZZTo4L_TuneCP5_13TeV_powheg_pythia8	1.212
	WZTo2L2Q_13TeV_amcatnloFXFX_madspin_pythia8	5.595
VVV	ZZZ_TuneCP5_13TeV-amcatnlo_pythia8	0.01398
	WZZ_TuneCP5_13TeV-amcatnlo_pythia8	0.05565
	WWZ_TuneCP5_13TeV-amcatnlo_pythia8	0.16510
	WWW_4F_TuneCP5_13TeV-amcatnlo_pythia8	0.18331
Non-Prompt	Data-driven (tight-to-loose method)	

Mass point	Cross-section [pb]
Scalar mediators	
DMscalar_Dilepton_top_tWChan_Mchi1_Mphi10	0.4632
DMscalar_Dilepton_top_tWChan_Mchi1_Mphi20	0.3021
DMscalar_Dilepton_top_tWChan_Mchi1_Mphi50	0.1236
DMscalar_Dilepton_top_tWChan_Mchi1_Mphi100	0.05262
DMscalar_Dilepton_top_tWChan_Mchi1_Mphi150	0.03173
DMscalar_Dilepton_top_tWChan_Mchi1_Mphi200	0.02204
DMscalar_Dilepton_top_tWChan_Mchi1_Mphi250	0.01627
DMscalar_Dilepton_top_tWChan_Mchi1_Mphi300	0.01240
DMscalar_Dilepton_top_tWChan_Mchi1_Mphi350	0.00951
DMscalar_Dilepton_top_tWChan_Mchi1_Mphi400	0.006274
DMscalar_Dilepton_top_tWChan_Mchi1_Mphi450	0.004236
DMscalar_Dilepton_top_tWChan_Mchi1_Mphi500	0.002995
DMscalar_Dilepton_top_tWChan_Mchi1_Mphi1000	0.0002844
Pseudoscalar mediators	
DMpseudoscalar_Dilepton_top_tWChan_Mchi1_Mphi10	0.05745
DMpseudoscalar_Dilepton_top_tWChan_Mchi1_Mphi20	0.05482
DMpseudoscalar_Dilepton_top_tWChan_Mchi1_Mphi50	0.0462
DMpseudoscalar_Dilepton_top_tWChan_Mchi1_Mphi100	0.03417
DMpseudoscalar_Dilepton_top_tWChan_Mchi1_Mphi150	0.02572
DMpseudoscalar_Dilepton_top_tWChan_Mchi1_Mphi200	0.01959
DMpseudoscalar_Dilepton_top_tWChan_Mchi1_Mphi250	0.01509
DMpseudoscalar_Dilepton_top_tWChan_Mchi1_Mphi300	0.01170
DMpseudoscalar_Dilepton_top_tWChan_Mchi1_Mphi350	0.007333
DMpseudoscalar_Dilepton_top_tWChan_Mchi1_Mphi400	0.004083
DMpseudoscalar_Dilepton_top_tWChan_Mchi1_Mphi450	0.002891
DMpseudoscalar_Dilepton_top_tWChan_Mchi1_Mphi500	0.002168
DMpseudoscalar_Dilepton_top_tWChan_Mchi1_Mphi1000	0.0002607

$t\bar{t}+DM$ signal samples

Mass point	Cross-section [pb]
Scalar mediators	
TTbarDMJets.Dilepton_scalar_LO_TuneCP5_13TeV-madgraph-mcatnlo-pythia8.mChi_1.mPhi_50	$3.405 \cdot 10^{-1}$
TTbarDMJets.Dilepton_scalar_LO_TuneCP5_13TeV-madgraph-mcatnlo-pythia8.mChi_1.mPhi_100	$8.027 \cdot 10^{-2}$
TTbarDMJets.Dilepton_scalar_LO_TuneCP5_13TeV-madgraph-mcatnlo-pythia8.mChi_1.mPhi_150	$2.673 \cdot 10^{-2}$
TTbarDMJets.Dilepton_scalar_LO_TuneCP5_13TeV-madgraph-mcatnlo-pythia8.mChi_1.mPhi_200	$1.158 \cdot 10^{-2}$
TTbarDMJets.Dilepton_scalar_LO_TuneCP5_13TeV-madgraph-mcatnlo-pythia8.mChi_1.mPhi_250	$6.020 \cdot 10^{-3}$
TTbarDMJets.Dilepton_scalar_LO_TuneCP5_13TeV-madgraph-mcatnlo-pythia8.mChi_1.mPhi_300	$3.579 \cdot 10^{-3}$
TTbarDMJets.Dilepton_scalar_LO_TuneCP5_13TeV-madgraph-mcatnlo-pythia8.mChi_1.mPhi_350	$2.376 \cdot 10^{-3}$
TTbarDMJets.Dilepton_scalar_LO_TuneCP5_13TeV-madgraph-mcatnlo-pythia8.mChi_1.mPhi_400	$1.443 \cdot 10^{-3}$
TTbarDMJets.Dilepton_scalar_LO_TuneCP5_13TeV-madgraph-mcatnlo-pythia8.mChi_1.mPhi_450	$9.025 \cdot 10^{-4}$
TTbarDMJets.Dilepton_scalar_LO_TuneCP5_13TeV-madgraph-mcatnlo-pythia8.mChi_1.mPhi_500	$6.204 \cdot 10^{-4}$
TTbarDMJets.Dilepton_scalar_LO_TuneCP5_13TeV-madgraph-mcatnlo-pythia8.mChi_20.mPhi_100	$7.993 \cdot 10^{-2}$
TTbarDMJets.Dilepton_scalar_LO_TuneCP5_13TeV-madgraph-mcatnlo-pythia8.mChi_30.mPhi_100	$8.052 \cdot 10^{-2}$
TTbarDMJets.Dilepton_scalar_LO_TuneCP5_13TeV-madgraph-mcatnlo-pythia8.mChi_40.mPhi_100	$8.147 \cdot 10^{-2}$
TTbarDMJets.Dilepton_scalar_LO_TuneCP5_13TeV-madgraph-mcatnlo-pythia8.mChi_45.mPhi_100	$8.319 \cdot 10^{-2}$
TTbarDMJets.Dilepton_scalar_LO_TuneCP5_13TeV-madgraph-mcatnlo-pythia8.mChi_49.mPhi_100	$8.304 \cdot 10^{-2}$
TTbarDMJets.Dilepton_scalar_LO_TuneCP5_13TeV-madgraph-mcatnlo-pythia8.mChi_51.mPhi_100	$9.735 \cdot 10^{-4}$
TTbarDMJets.Dilepton_scalar_LO_TuneCP5_13TeV-madgraph-mcatnlo-pythia8.mChi_55.mPhi_100	$4.835 \cdot 10^{-4}$
Pseudoscalar mediators	
TTbarDMJets.Dilepton_pseudoscalar_LO_TuneCP5_13TeV-madgraph-mcatnlo-pythia8.mChi_1.mPhi_50	$3.440 \cdot 10^{-2}$
TTbarDMJets.Dilepton_pseudoscalar_LO_TuneCP5_13TeV-madgraph-mcatnlo-pythia8.mChi_1.mPhi_100	$2.164 \cdot 10^{-2}$
TTbarDMJets.Dilepton_pseudoscalar_LO_TuneCP5_13TeV-madgraph-mcatnlo-pythia8.mChi_1.mPhi_150	$1.414 \cdot 10^{-2}$
TTbarDMJets.Dilepton_pseudoscalar_LO_TuneCP5_13TeV-madgraph-mcatnlo-pythia8.mChi_1.mPhi_200	$9.773 \cdot 10^{-3}$
TTbarDMJets.Dilepton_pseudoscalar_LO_TuneCP5_13TeV-madgraph-mcatnlo-pythia8.mChi_1.mPhi_250	$6.753 \cdot 10^{-3}$
TTbarDMJets.Dilepton_pseudoscalar_LO_TuneCP5_13TeV-madgraph-mcatnlo-pythia8.mChi_1.mPhi_300	$4.808 \cdot 10^{-3}$
TTbarDMJets.Dilepton_pseudoscalar_LO_TuneCP5_13TeV-madgraph-mcatnlo-pythia8.mChi_1.mPhi_350	$2.742 \cdot 10^{-3}$
TTbarDMJets.Dilepton_pseudoscalar_LO_TuneCP5_13TeV-madgraph-mcatnlo-pythia8.mChi_1.mPhi_400	$1.409 \cdot 10^{-3}$
TTbarDMJets.Dilepton_pseudoscalar_LO_TuneCP5_13TeV-madgraph-mcatnlo-pythia8.mChi_1.mPhi_450	$9.302 \cdot 10^{-4}$
TTbarDMJets.Dilepton_pseudoscalar_LO_TuneCP5_13TeV-madgraph-mcatnlo-pythia8.mChi_1.mPhi_500	$6.618 \cdot 10^{-4}$
TTbarDMJets.Dilepton_pseudoscalar_LO_TuneCP5_13TeV-madgraph-mcatnlo-pythia8.mChi_20.mPhi_100	$2.166 \cdot 10^{-2}$
TTbarDMJets.Dilepton_pseudoscalar_LO_TuneCP5_13TeV-madgraph-mcatnlo-pythia8.mChi_30.mPhi_100	$2.164 \cdot 10^{-2}$
TTbarDMJets.Dilepton_pseudoscalar_LO_TuneCP5_13TeV-madgraph-mcatnlo-pythia8.mChi_40.mPhi_100	$2.162 \cdot 10^{-2}$
TTbarDMJets.Dilepton_pseudoscalar_LO_TuneCP5_13TeV-madgraph-mcatnlo-pythia8.mChi_45.mPhi_100	$2.180 \cdot 10^{-2}$
TTbarDMJets.Dilepton_pseudoscalar_LO_TuneCP5_13TeV-madgraph-mcatnlo-pythia8.mChi_49.mPhi_100	$2.151 \cdot 10^{-2}$
TTbarDMJets.Dilepton_pseudoscalar_LO_TuneCP5_13TeV-madgraph-mcatnlo-pythia8.mChi_51.mPhi_100	$1.993 \cdot 10^{-3}$
TTbarDMJets.Dilepton_pseudoscalar_LO_TuneCP5_13TeV-madgraph-mcatnlo-pythia8.mChi_55.mPhi_100	$7.750 \cdot 10^{-4}$

References I

-  J. Woithe, G.J. Wiener and F. Van der Vecken, "Let's have a coffee with the Standard Model of particle physics!", Physics education 52, number 3, 2017
-  F. Zwicky, "Die Rotverschiebung von extragalaktischen Nebeln", Helvetica Physica Acta , vol. 6, pp. 110-127, 1933
-  K.G. Begeman, A.H. Broeils and R.H. Sanders, "Extended rotation curves of spiral galaxies - Dark haloes and modified dynamics", Monthly Notices of the Royal Astronomical Society, vol. 249, issue 3, ISSN 0035-8711, 1991
-  D.J. Fixsen, "The temperature of the cosmic microwave background", Astrophysical Journal, 2009
-  L. Heurtier, H. Partouche, "Spontaneous Freeze Out of Dark Matter From an Early Thermal Phase Transition", CPHT-RR065.112019 [arXiv: 1912.02828]
-  D. Clowe et all., "A Direct Empirical Proof of the Existence of Dark Matter", Astrophysical Journal Letters 648, 2006

References II

-  CMS Collaboration, "Search for dark matter particles produced in association with a top quark pair at $\sqrt{s} = 13$ TeV", Phys. Rev. Lett. 122, 011803 (2019) [arXiv: 1807.06522]
-  CMS Collaboration, "Search for dark matter produced in association with a single top quark or a top quark pair in proton-proton collisions at $\sqrt{s} = 13$ TeV", JHEP, vol. 03 141, 2019 [arXiv: 1901.01553]
-  S. Chatrchyan et al., "Observation of a new boson at a mass of 125 GeV with the CMS experiment at the LHC", Phys. Lett. B716, pp. 30-61, 2012 [arXiv: 1207.7235]
-  G. Aad et al., "Observation of a new particle in the search for the Standard Model Higgs boson with the ATLAS detector at the LHC", Phys. Lett. B716, pp. 1-29, 2012 [arXiv: 1207.7214]
-  CMS Twiki, "Top + DM Run II Legacy analysis", <https://twiki.cern.ch/twiki/bin/viewauth/CMS/TopPlusDMRunIILegacy>